PCCP

PAPER

View Article Online
View Journal | View Issue

Cite this: *Phys. Chem. Chem. Phys.*, 2016, **18**, 26923

Complexes of Ni(II) and Cu(II) with small peptides: deciding whether to deprotonate†

Robert C. Dunbar,*[a] Jonathan Martens,*[b] Giel Berden[b] and Jos Oomens*[bc]

Received 7th June 2016,
Accepted 8th September 2016

DOI: 10.1039/c6cp03974j

www.rsc.org/pccp

The observed variety of metal-ion complexation sites offered by peptides reflects a basic tension between charge solvation of the ion by Lewis-basic chelating groups *versus* amide nitrogen deprotonation and formation of metal–nitrogen bonds. Gas-phase models of metal-ion coordination can illuminate the factors governing this choice in condensed-phase proteins and enzymes. Here, structures of gas-phase complexes of Ni(II) and Cu(II) with tri- and tetra-peptide ligands are mapped out using a combination of Infrared Multiple Photon Dissociation (IRMPD) spectroscopy and density functional theory (DFT) computations. The two binding modes give distinctive IRMPD signatures, particularly in the diagnostic region 1500–1550 cm^{-1}. Previous observations have suggested that Ni(II) complexes preferentially show the iminol rearrangement pattern (Im) giving low-spin square-planar geometries with metal-ion bonds to deprotonated amide nitrogens. In contrast, alkaline earth metal ion complexes prefer amide carbonyl oxygens chelating the metal ion with pyramidal geometry (charge-solvation, CS). Surprisingly, it is shown here that the Gly_4 complexes are CS bound, in contrast with the expectation of Im binding. It is suggested that CS binding is actually a normal Ni(II) and Cu(II) binding mode to simple peptides lacking participating side chains. Three factors are suggested to influence the choice between CS and Im binding patterns: (1) presence of an accessible side-chain Lewis-basic proton interaction site (FGGF, FGG and HAA complexes); (2) short chain length of the peptide leading to a shortage of accessible carbonyl oxygen sites for CS binding, (AAA, FGG and HAA complexes); (3) outright deprotonation of the ligand giving net negatively charged $Im[Ni^{2+}(Gly_4–3H^+)]^-$ and $Im[Ni^{2+}(Ala_3–3H^+)]^-$ complexes, which have a triply-deprotonated ligand. IRMPD spectra of $[Cu^{2+}Gly_4]^{2+}$ and $[Cu^{2+}(Gly_4–3H^+)]^-$ complexes suggest that their structures are similar to their Ni^{2+} analogs.

1. Introduction

An increasing body of knowledge about gas-phase metal-ion complexation by peptide ligands is developing thanks to the emergence of ever more powerful experimental and computational tools. Nevertheless, this gas-phase effort remains substantially isolated from the far larger body of knowledge regarding metal-ion interactions with small-molecule ligands, such as peptides, proteins, and enzymes in condensed phases. Peptide complexation with transition metals provides a particularly rich playground for making correlations and comparisons between gas-phase and condensed-phase complex characteristics.

In condensed phases, nickel ions are well known for their tendency to complex Lewis-basic ligands in a square-planar tetradentate array of deprotonated nitrogens, oxygens and other basic chelation sites, and this binding pattern has been found also to characterize a number of gas-phase Ni(II) and Cu(II) complexes.[1–5] It was thus startling to find here, that the tetra-glycine ligand, which offers a virtually textbook opportunity for square-planar nitrogen-based complexation, actually prefers to bind *via* a pyramidal cage based on its carbonyl oxygens. This paper reports our progress towards understanding this unexpected finding through comparison with other small peptide nickel-ion ligands whose gas-phase behavior parallels the condensed-phase expectation of square-planar nitrogen-based caging of the nickel ion.

Recent and powerful techniques, including ion mobility spectrometry,[6] IR spectroscopy, UV spectroscopy, H/D exchange,[7] FRET fluorescence[8] and a variety of computational techniques

[a] *Chemistry Department, Case Western Reserve University, Cleveland, Ohio 44106, USA. E-mail: rcd@po.cwru.edu*
[b] *FELIX Laboratory, Institute for Molecules and Materials, Radboud University, Toernooiveld 7c, 6525ED Nijmegen, The Netherlands. E-mail: jonathan.martens@science.ru.nl*
[c] *University of Amsterdam, Science Park 904, 1098XH Amsterdam, The Netherlands. E-mail: joso@science.ru.nl*

† Electronic supplementary information (ESI) available: 1. Full citation for Frisch *et al.*, ref. 83. 2. Comparative structure plots for Ni(II) and Cu(II) complexes discussed in the text (PDF). Figure captions noting normal mode characters of diagnostic calculated IR peaks. Enlarged figure plots are provided for the nickel isomeric structures presented in the spectral figures. Coordinates for all the optimized structures mentioned in the paper are available on request from the first author. See DOI: 10.1039/c6cp03974j

have supplemented the traditional structure-probing approach *via* interpretation of mass spectrometric fragmentation pathways, to open a wealth of new structural information on gas-phase systems. The present work focuses on IR-spectroscopic experiments coupled with density functional theory (DFT) computations in the study of metal-ion complexes of peptides. Examples of related recent work using spectroscopic approaches in such systems include IR spectroscopy on metal-complexed peptide cations,[1–5,9–29] anions[23,30–32] and proteins,[23,31,33] and UV spectroscopy of peptide and protein complexes.[30,34–43] Similar experimental methods have been applied to protonated peptides and proteins, and we can note a few representative studies of protonated species[14,39–41,43–59] and some relevant general reviews of ion spectroscopy-based approaches.[60–64]

Incorporation of metal ions by peptide and protein partners characteristically involves chelation of the metal ion at several Lewis-basic sites drawn both from the amide linkages and the amino acid side chains. In general, there are many ways for a metal-binding pocket to form in a peptide. Amide linkages provide a rich supply of strongly Lewis-basic sites which normally participate in the metal-ion binding; a choice is generally made between chelation by the amide carbonyl oxygens, known as charge-solvation (CS) binding, or alternatively deprotonation of amide nitrogens and chelation by direct metal–nitrogen bonds[5,17,65] (see Fig. 1). The CS motif is characteristic of alkali metal ions and Ca^{2+} and Mg^{2+} ions, whereas the second motif is considered to be characteristic of more active metal ions like Co^{2+}, Ni^{2+}, Cu^{2+}, Zn^{2+}, Pd^{2+} and Cd^{2+}. The CS motif, for example, characterizes calcium transporter proteins like calmodulin.[66] A well-known example of the second motif having particular relevance here is the ATCUN (amino terminal Cu(II)- and Ni(II)) structural pattern,[67–71] originally studied in human serum albumin, but now known to recur in a wide variety of proteins. Other examples of nitrogen backbone binding can be seen in the binding of metal ions in oxytocin[72] and the binding of Cu(II) in the prion protein.[73–75]

To address the factors in the competition between CS and Im binding preferences, and to map out connections between gas-phase and condensed-phase observations, we focus on nickel(II) as a particularly well studied and rich example. This ion shows interesting gas-phase complexation variations and is also the subject of a vast body of literature addressing its solution and solid-state complexation in both organometallic contexts and biologically relevant peptide, protein and enzyme contexts.[17,68,69,76–81]

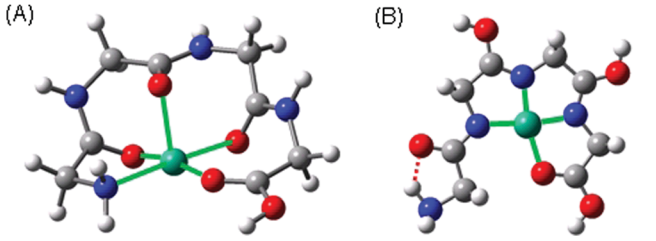

Fig. 1 Conceivable Ni(II) ion binding patterns for Gly_4: (A) CS binding (CS[OOOON]) to the carbonyl oxygens along with the terminal amino nitrogen (green bonds); (B) iminol binding (Im[NNNO]) to the deprotonated amide nitrogens and the carboxyl carbonyl (green bonds). The Ni^{2+} ion is colored green.

In an unrearranged peptide, metal-ion binding at amide nitrogens is blocked by amide protons. Early on, it was thought that a metal ion might bind amide nitrogens by expanding the nitrogen coordination and sharing the nitrogen site with the hydrogen, but this possibility came to be discounted,[82] and deprotonation is recognized as a prerequisite to metal-ion–nitrogen bond formation. For peptides in condensed-phase environments, deprotonation of a backbone amide nitrogen is accomplished by removal of the proton into the solvent background at higher pH, or onto remote basic sites in a large peptide. Such a displacement of the amide proton means that metal ions such as Ni(II) and Cu(II), which form strong metal to amide–nitrogen bonds, can readily induce amide–nitrogen deprotonation in crystals or solutions. However, for isolated peptide complexes in the gas phase, attachment of the metal cation to a backbone nitrogen must pay an energy cost to accommodate the displaced proton locally or pull it free from the complex altogether. Previously, our work with these systems has focused on the iminol tautomerization as a viable way of relocating this proton away from the amide nitrogen onto the amide oxygen to give the iminol (Im) binding mode (Fig. 1(B)).[2–4] Experimental and computational studies of small-peptide complexes have found the Im deprotonated nitrogen binding mode to be preferred over CS binding for Ni(II) (as well as Cu(II)). It was thus unexpected, upon observing the complexes with tetraglycine presented here, to find that CS binding is preferred with this particular ligand. This observation suggests a new perspective, based on the premise that CS binding is a viable gas-phase peptide binding mode for Ni(II) just as it is for less active metal ions like Mg(II) and Ca(II), and that conversion to deprotonated nitrogen binding of Ni(II) must be induced by some extra encouragement. Here we show examples of deprotonated-nitrogen binding of Ni(II) contrasting with the CS binding observed for tetraglycine. We suggest three factors which can encourage binding by amide–nitrogen deprotonation and can account for a switch from CS to Im binding: (a) stabilization of the iminol-rearranged form of the peptide by H-bonding of the iminol proton to a basic side chain, (b) relative destabilization of the CS isomer due to a deficit of C=O chelation sites in very small peptides; and (c) outright brute-force removal of the interfering amide protons giving overall negatively charged complexes.

In the present report, following a discussion of the CS character of the $NiGly_4^{2+}$ complex, the three suggested ways will be described by which a switch to the Im binding mode can be induced. First, side-chain H-bonding is illustrated with the Ni^{2+}HAA, Ni^{2+}FAA and Ni^{2+}FGGF examples; second, shortage of CO chelation points is illustrated with the $NiAAA^{2+}$ example as well as the other two already-mentioned tripeptides; third, outright deprotonation is illustrated with the $[Ni^{2+}(Ala_3–3H^+)]^{-1}$ and $[Ni^{2+}(Gly_4–3H^+)]^{-1}$ complexes. Finally, corresponding Cu^{2+} complexes are shown to emphasize the close similarity of Cu(II) and Ni(II) gas-phase complexation behavior. One recurring theme is

the exceptionally useful marker for distinguishing CS *versus* Im binding which is provided by the presence or absence of vibrational intensity in the 1500–1550 cm^{-1} region characteristic of the amide II peptide vibrational mode (N–H bend plus C–N stretch).

2. Methods

Structure notation

A descriptive structure notation is used (for example, CS[OOOON] or Im[NNNO] as in Fig. 1). The binding type is indicated (CS = charge solvated; Im = iminol; Im2CS1 = two iminol and one CS amide; or ZW = carboxylate zwitterion). Following in brackets is the set of metal-bound chelation points. Deprotonated amide nitrogens are given first (N), then carbonyl oxygens (O), then N-terminal amino nitrogen (N), and finally ring (R) (either imidazole nitrogen or π-complexed phenyl).

Computation

All the calculations were carried out using the Gaussian09 quantum chemical package.[83] Density functional theory (DFT) calculations at the B3LYP/6-31+G(d,p) level served as the default computational methodology. For the comparison of the relative energies separating various isomers, differences of less than 20 kJ mol^{-1} were considered important for the present purposes and were normally verified using the larger 6-311++G(d,p) basis set. The two different basis sets usually gave differences in relative energies in agreement within a few kJ mol^{-1}, and seldom disagreed by more than 5 kJ mol^{-1}. By this criterion, we have considered the smaller basis set large enough for reliable energy comparisons (to the extent of validity of the B3LYP functional) within the present universe of complexes, but the larger basis set was used to verify energy comparisons of the most important conformations. Ni(II) complexes were calculated with singlet (low-spin) and triplet (high spin) spin states, while Cu(II) was calculated only with doublet spin state. Vibrational zero-point energy corrections and calculations of 298 K free energies were made at the highest used computational level for each isomer, assuming a harmonic-oscillator/rigid-rotor model for vibrational thermochemical effects. For comparison of DFT-calculated spectra to experimental IRMPD spectra, the computed frequencies were scaled by a factor of 0.965 (0.975 for the larger basis set), which was considered consistent with the range of scaling factors used in recent work on small peptide systems at these levels of theory.[3,84,85] Computed spectra were convoluted with a 20 cm^{-1} FWHM Gaussian lineshape function for comparison to experimental IRMPD spectra.

Drawing on our prior experience with transition-metal/peptide complex structures and known structural motifs found in the condensed-phase literature, initial guess structures for DFT optimization were generated by manual definition of chemically sensible conformations considered to be low-energy candidates. The powerful structure-determining influence of nickel or copper ion chelation constrains the array of reasonable structures to a manageable level.

The present study is not aimed at producing an in-depth description of the thermochemistry of these species. but rather at determining structural binding motifs based on comparison of IRMPD spectra with DFT calculated IR spectra. We have selected the B3LYP functional for this study based on the large body of work demonstrating the appropriate use of this functional for the calculation of IR spectra in general as well as specifically for peptide–metal ion complexes. We note that various other functionals for Ni(II)[86,87] and corrections for dispersion[88,89] have been suggested in order to obtain accurate energetics.

The $Ni^{2+}Gly_4$ complex has particular interest here. The CS-bound structures of this complex are definitely high spin, while the Im structures are low-spin. A number of trials were made on this system with various computational protocols. Trials with DFT (varying bases and functionals including B3LYP, MPW1PW91, M06, OPBE), as well as with MP2, were made. Two dispersion corrections (GD3[89] and GD3BJ[88]) were tried for $NiGly_4$ (and also NiFGGF). These various computational protocols yielded wide variations in magnitude and even sign of the relative energies of the CS and Im structures. The computed spectra for different calculation protocols consistently showed the amide II marker peak to be a reliable indicator of CS binding conformation. Beyond this, it was our conclusion that for such predictions of relative energies, we do not have confidence in any one of these protocols, and we cannot undertake to decide which would be most reliable. In general, the unimproved B3LYP functional with modest basis sets has in past work given us and other workers sensible energy comparisons, usually in good accord with spectroscopic experimental determinations of the ground state (for a few examples, see ref. 1–3, 90 and 91). The recent literature gives some encouraging examples of the application of unimproved B3LYP to such singlet/triplet energy comparisons of Ni(II) complexes with apparently satisfactory results, for instance ref. 92–94. Accordingly, we present simple B3LYP energetics as a useful guide to trends, and point to our experimental evidence as the most reliable source of information about the singlet/triplet choice of ground states at our present stage of computational capability.

IRMPD experimental

IR spectra of the gaseous metal ion–peptide complexes were recorded employing a modified quadrupole ion trap mass spectrometer (Bruker, Amazon Speed ETD) or a home built Fourier-transform ion cyclotron resonance (FT-ICR) mass spectrometer, both coupled to the Free Electron Laser for Infrared eXperiments (FELIX) as has been detailed elsewhere.[17,63,95] In both setups, metal-ion peptide complexes were generated by electrospray ionization from solutions containing the peptide and metal salt in acetonitrile/H_2O ($\sim$4 : 1). Target ions were trapped, mass-selected and irradiated with the wavelength-tunable infrared light from FELIX. By plotting the sum of all dissociation channels ratioed to the total ion count as a function of laser frequency, an infrared action spectrum was generated and interpreted as a surrogate IR spectrum of the complex. DFT computed linear absorption IR spectra of candidate ion structures were compared with the observed spectra for structure assignment, and the

calculated relative energetics provided additional guidance to assign conformational and tautomeric structures.

In the following discussions, we report on results for Gly_n complexes and corresponding Ala_n complexes interchangeably. This Gly/Ala equivalence seems very reasonable, and is supported by a high degree of energetic and structural equivalence in a number of computational comparisons in both published and unpublished work from this laboratory. The choice between Gly and Ala chains in our experiments has been governed by experimental convenience (commercial availability).

3. Results and discussion

Identifying factors governing whether a complex does or does not undergo iminol rearrangement was addressed using seven illustrative IRMPD spectra, which are displayed together in Fig. 2. The principal diagnostic spectral feature for rearrangement is the disappearance of the amide II vibrational mode, conveniently located in the otherwise uncluttered region between about 1520 and 1580 cm^{-1}, as highlighted in color in the figure. This mode is largely dominated by bending motion of the amide N–H proton(s), which is (are) absent in the iminol-rearranged conformation.

In previous structure assignments based on IRMPD spectra, peptide complexes of Ni(II) have always been assigned as forming iminol structures.[1–5] It was thus surprising and interesting to find that the $Ni^{2+}Gly_4$ complex has a distinctively different spectral pattern than all these other (iminol) examples and that in this unique case the complex clearly adopts a CS structure (Fig. 3). The experimental IRMPD spectrum shows excellent agreement with the computed spectrum for a CS coordination structure (CS[OOOON]),

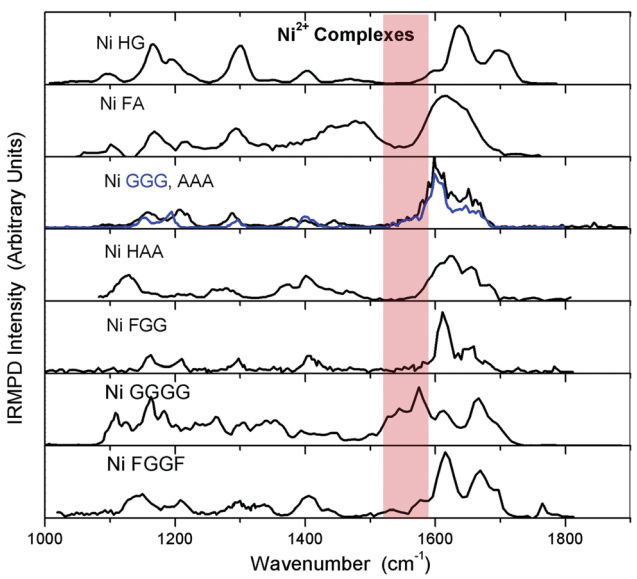

Fig. 2 IRMPD spectra of the complexes illustrated in this study. The highlighted area shows the region of the characteristic amide II band that differentiates CS binding from deprotonated nitrogen (Im) binding. Judging on this basis, all of the complexes displayed are predominantly Im, except Ni GGGG, which is predominantly CS.

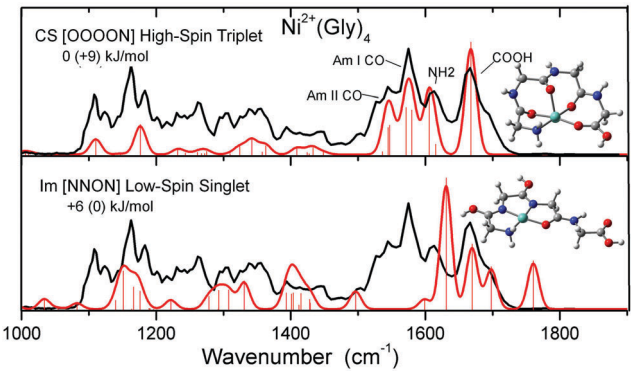

Fig. 3 (upper) Ni^{2+} Gly_4 IRMPD spectrum (black) and the predicted spectrum for the pentacoordinate CS structure (red). The most distinctive CS features are the amide II vibrational modes between about 1500 and 1550 cm^{-1}. (lower) Similar comparison with the predicted spectrum for the lowest-energy iminol-rearranged structure. Calculated energies are given in kJ mol^{-1} (free energies in parentheses) relative to the lowest-energy structure that was located for the given complex. Further comparisons with predicted spectra of possible alternative structures are shown in the ESI,† Fig. S1. Note that enlarged pictures of all the structures mentioned are also included in the ESI† figures for easier viewing.

and very poor agreement with the lowest-energy iminol-rearranged structure (Im2CS1[NNON]) or the fully-rearranged iminol structures (Im3[NNNN] and Im3[NNNO]), all shown in Fig. S1 (ESI†). The unexplained shoulder at 1700 cm^{-1} in the IRMPD spectrum suggests some presence of another structure, which could be one of those shown in Fig. S1 (ESI†), or another structure not yet identified. The richness of the spectrum in the 1100–1200 cm^{-1} range similarly suggests the likely co-existence of a minor fraction of another structure in addition to CS[OOOON].

The exceptional nature of the Gly_4 complex is reasonably consistent with the thermochemistry as well. As an adjunct to the relative conformer energies displayed in the figures, Table 1 collects the comparative energies of the best iminol *versus* the best CS complexes for the series of complexes studied in this report. As the table indicates, the CS structure for the Gly_4 complex is considerably more stable (by more than 40 kJ mol^{-1}) than the iminol Im3 alternatives (Im3[NNNO], Im3[NNNN] or Im3[NNNON]) having all three amide nitrogens deprotonated and bound to the metal (see Fig. S1, ESI† for structures). Interestingly, in the Gly_4 case, the deprotonation of only two of the three available

Table 1 Relative energies of the two or three possible low energy conformation types for the indicated ligands of the Ni(II) complexes. Energies are relative to the lowest energy structure that we located. Free energies at 298 K given in parentheses. Fully optimized B3LYP with 6-311++G(d,p) basis (kJ mol^{-1})

	CS	Iminol (Im2CS1)	Iminol (Im3)
HG	36	—	0
FA	36 (+35)	—	0 (0)
AAA	+46 (+46)	—	0 (0)
HAA	+52 (+49)	—	0 (0)
FGG	+35 (+34)	—	0 (0)
GGGG	0 (+9)	+6 (0)	+46 (+32)
FGGF	+8 (+13)	0 (0)	+57 (+59)

amide linkages, to give the square-planar singlet structure designated Im2CS1, is considerably more favorable than the Im3 structures. This structure, which is displayed with its predicted spectrum in Fig. 3, is only slightly inferior to the fully CS structure (by 6 kJ mol^{-1} on an energy basis), and may actually be narrowly predicted as the most favorable structure on a free-energy basis, but there is no sign of its presence in the IRMPD spectrum, particularly indicated by the absence of any feature around 1760 cm^{-1}. As discussed below, this last structure motif (Im2CS1) is actually the ground state calculated and observed for the FGGF complex.

Having shown that the simple tetrapeptide ligand Gly_4 gives a clear, if unexpected, CS complex, we move to consideration of examples having the expected Im binding pattern, illustrating three factors which apparently enhance amide–nitrogen deprotonation and amide–nitrogen-to-metal binding.

(a) Iminol stabilization by basic side chains

One way to drive the iminol-mediated deprotonation of the amide nitrogens is to provide a sufficiently basic interaction for one or more of the iminol protons through proximity to a Lewis-basic site on a side chain. Three examples are shown in Fig. 4, in each of which an interaction of one of the iminol protons with a Lewis-basic side chain provides a measure of stabilization of the iminol-rearranged form leading to a ground state having Im bonding of the complex. For HAA and FGG the ground states shown each have a straightforward stabilizing interaction of an iminol OH group, *i.e.* a normal hydrogen bond in the former, and a cation–π interaction in the latter. The ground state of the FGGF complex is more surprising: calculations suggest that the full threefold iminol rearrangement structure (Im NNNO) is unfavorable (Table 1 and Fig. S2, ESI†), but the partial iminol rearrangement involving two of the three amide linkages to give the Im2CS1[NNON] structure, as shown in Fig. 4, is now the most favorable of all. In particular, the cation–π interaction of the iminol proton with the N-terminal phenyl group provides driving force toward rearrangement, but the possibility of the good hydrogen bond shown between the C-terminal amide proton of the unrearranged amide and the carboxyl oxygen evidently discourages the iminol rearrangement of this third amide linkage.

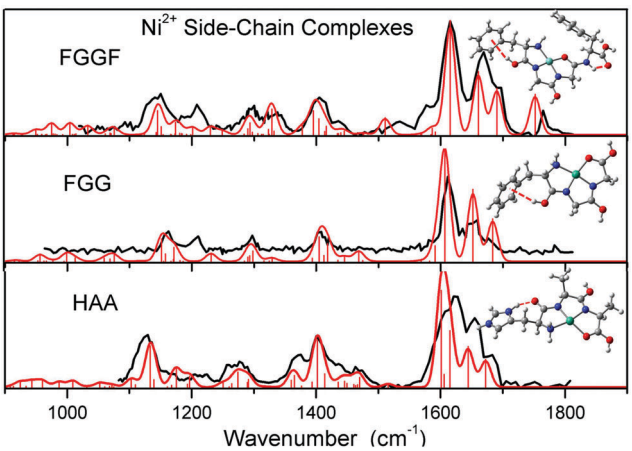

Fig. 4 Computed spectra (red) and IRMPD spectra (black) of the Im-type ground states of the Ni(II) complexes of FGGF, FGG and HAA. Stabilizing interactions of an iminol proton are seen in all three cases (cation–pi interaction for FGGF and FGG, hydrogen bonding N···H···O interaction for HAA). The unusual mixed-character Im2CS1[NNON] conformation of the Ni(II) complex for FGGF is enforced by the excellent additional O···H···N hydrogen bond involving the unrearranged C-terminal amide linkage.

(b) Iminol stabilization through the exceptional nature of small peptide ligands

Short simple peptides (like dialanine and trialanine) are exceptional in forming iminol ground states, in contrast to the CS complex formed with tetraglycine. The trend of relative energies is shown in Table 1. Simple di- and tripeptide ligands are inadequate models for metal ion coordination by longer peptides (tetrapeptide and beyond), because the former have too few carbonyl chelation points to fully enclose the metal atom in a CS cage comparable to protein environments.

In the series of Ni(II) complexes with Ala_2, Ala_3 and Gly_4, a switch from Im to CS between Ala_3 and Gly_4 is qualitatively rationalized (in an admittedly oversimplified argument) by counting the number of available metal chelation points. The low-spin iminol structures are square-planar with four strong bonds to the metal, while the high-spin CS structures are able to accommodate up to six coordination points. With Ala_2 and with Ala_3, Im and CS structures can provide equal numbers of metal-coordinated atoms without undue steric strain (three for Ala_2, four for Ala_3), so the Im structure (which includes more strong metal–nitrogen bonds) wins out over the CS structure (which has a greater fraction of weaker[96] metal–oxygen bonds). On the other hand, Gly_4 can comfortably provide five coordinated atoms in the CS structure, which is preferable to the four coordinated atoms in the Im structure. (The Gly_4 and Ala_3 structures are displayed in Fig. S1 and S3 (ESI†), while the calculated structure of $Ni^{2+}Ala_2$ was described previously.[2])

The Ala_2 complexes of Ni(II) and Cu(II) have not yet been experimentally accessible, but the Im preference of the Ni(II) Ala_3 complex is plainly evident from the spectrum in Fig. 5. The calculated spectrum for Im[NNON] accounts well for nearly all

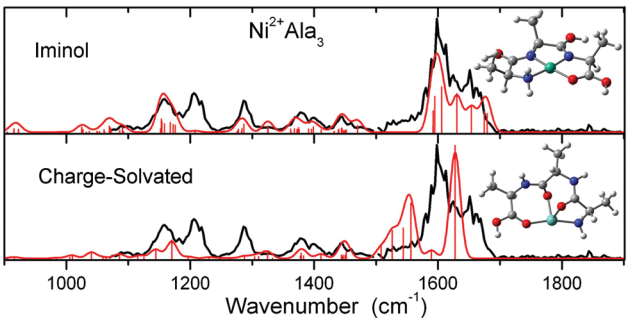

Fig. 5 Computed spectra (red) of the Im NNON conformation (upper) and the CS[OOON] conformation (lower) of the Ala_3 complex of Ni(II) compared with the IRMPD spectrum (black). (The computed iminol spectrum of Im[NNON] is an average of the two low-lying iminol structures displayed in Fig. S3, ESI.†)

the observed peaks, and indicates at least a major contribution of this structure to the population. Note that alone among the complexes discussed in this report, a full match to the experimental spectrum could not be achieved for any one of the calculated structures (although the Im character of the spectrum is not in question). However, a mixture of equal fractions of the spectra of the two low-lying predicted singlet Im conformations gave the acceptable match displayed in Fig. 5. The separate spectra of the different predicted Im structures are shown in Fig. S4 (ESI†). (Im[NNON] and Im[NNON] Alt were combined to produce the plot given in Fig. 5). In addition, the unpredicted peak at 1210 cm^{-1} and the unexpected intensity around 1630 cm^{-1} suggest a possible contribution from yet a third conformer, which we have not been able to identify. The lack of observed intensity in the 1500–1550 cm^{-1} region is highly diagnostic for the absence of CS structures in the ion population (see Fig. S3, ESI†). The shift in binding motif from Im to CS upon going from Ala_3 to Gly_4 is further highlighted in Fig. S4 (ESI†) which juxtaposes the spectra for tripeptide and tetrapeptide complexes.

Two of the examples shown in Fig. 4 illustrate the combined result of both of the effects discussed so far, namely (a) side-chain interactions, and (b) small-peptide effect. These two examples are the tripeptide ligands FGG (Fig. 4 and Fig. S5, ESI†) and HAA (Fig. 4 and Fig. S6, ESI†) which have phenyl and imidazole side-chain groups, respectively, that are among the common Lewis-basic chelating groups in metal ion encapsulation. These two active-side-chain peptides have the same number of potential Lewis-basic chelation sites (five) as $(Gly)_4$, and their complexes with Ni^{2+} offer the possibility of five-coordinate CS solvation similar to $Ni^{2+}Gly_4$ (see Fig. S5 and S6, ESI† for these CS[OOONR] structures). However, two factors both act to disfavor the CS alternative. As noted in section (a) above, the basic side chains act as H-bond acceptor sites giving stabilization to the Im coordination motif. In addition, the limited tripeptide chain length leads to crowding and geometrical strain in the pentacoordinate CS structures. The sum of these two effects pushes both complexes strongly to an Im ground-state conformation.

In the case of HAA, the hydrogen-bonding interaction of the iminol proton with the imidazole ring is so strong that the best harmonic-oscillator description of the conformation shifts the proton to the imidazole nitrogen in a zwitterionic geometry (Fig. 4 and Fig. S6, ESI†). (In this example, the transfer of the proton from the transient O–H···N form to the deeper O···H–N potential energy well is spontaneous, and is estimated as energetically downhill by about 25 kJ mol^{-1}). In both of these examples, the most stable CS structure (Table 1) is the OOOR structure formed by opening up the pentacoordinate structure to tetracoordinate geometry, but this structure is not the ground state in either case.

Inspection of the IRMPD spectra in Fig. 4 immediately shows that all three of these complexes feature iminol-type binding. The key diagnostic feature is the absence of the amide II peak in the 1500–1550 cm^{-1} frequency range that would be characteristic of a CS structure. Adding strength to these assignments are a number of peaks predicted for the assigned ground state which are matched by peaks in the observed spectrum. These fitted peaks can be seen in the figures in the ESI.† In addition, in the captions to the ESI† figures are given normal mode characterizations of all of the predicted peaks which seem to have useful diagnostic value for assigning the ground state structures of the IRMPD spectra.

Somewhat to our surprise but reinforced by the computed thermochemistry, we observe for HAA (Fig. S6, ESI†) that the Im[NNON] conformation is preferred over alternatives that bind the imidazole nitrogen to the metal ion, namely Im[NNOR], CS[OOOR] or CS[OOONR]. This contrasts with the common observation of imidazole-to-metal binding in condensed-phase complexation of histidine-containing ligands, where the imidazole group always stabilizes the complex by direct chelation of the metal ion. The gas-phase situation is dominated by different considerations from the role of histidine anchors in condensed-phase cage formation. The remote Lewis-basic hydrogen-bonding site offered by the non-metal-bound imidazole residue in the gas-phase conformation is so strongly attractive to an iminol proton that it can draw this proton away, resulting in the final formation of the deprotonated-nitrogen iminol chelation that we display as the ground state in Fig. 4 and Fig. S6 (ESI†). As the figures indicate, this indirect mechanism of iminol stabilization still results in a good square-planar, low-spin tetradentate coordination of the nickel ion. The strongly hydrogen-bonded protonated-imidazole proton (Fig. 4 and Fig. S6, ESI†) might be best described as a shared proton.[16,97,98]

(c) Amide nitrogen binding stabilized through removal of the amide protons by outright deprotonation

Removing three protons from the di-cations discussed so far gives the mono-anions $[M^{2+}(peptide–3H^+)]^-$. The production of such complexes of late transition metal ions by electrospray ionization is well known,[72,96] (as are dianions with four protons removed[37]). The resulting triply deprotonated complex is precisely analogous to the condensed-phase structures with the metal bound to deprotonated amide nitrogens, and the gas-phase process should yield square planar complexes with the metal ion bound to up to three amide nitrogens along with additional coordinated atoms. Although there has been no reason to doubt this expectation for the gas-phase ions, spectroscopic evidence presented here for Ala_3 and Gly_4 (Fig. 6) adds strong confirmation that all of the amide linkages are indeed deprotonated and nitrogen-bound to the metal. For $Im[Ni^{2+}(Gly_4–3H^+)]^-$ this structure is nicely confirmed, as shown by the analysis of the IRMPD spectrum in Fig. S7 (ESI†). The alternative structures Im2CS1[NNON] with only two deprotonated amide nitrogens, and Im[NNNO] with the fourth chelation site occupied by the carboxyl O rather than the amino N, are considerably higher in energy and do not give good agreement between predicted and observed spectra. All high-spin (triplet) complexes that were explored gave much higher energies compared with the assigned low-spin square-planar structures.

Inspection of the spectrum of the $[Ni^{2+}(Gly_4–3H^+)]^-$ ion in Fig. 6, indicates that the two modes in the 1450 to 1600 cm^{-1} region of the Im[NNNN] ground state are calculated as well-separated bands at the calculated resolution, but appear to be

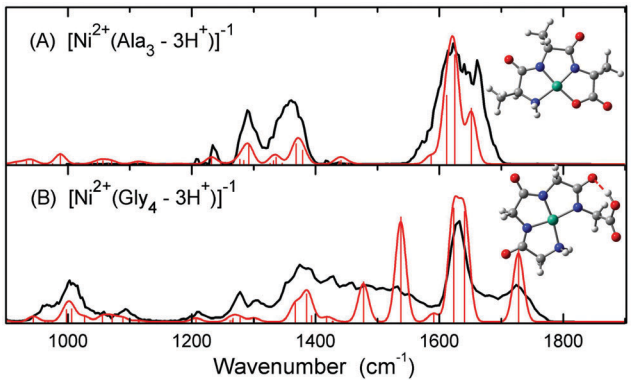

Fig. 6 IRMPD spectra (black) of triply deprotonated anions, along with computed spectra (red) of the best-fit structures from DFT calculations. (A) Im[$Ni^{2+}(Ala_3-3H^+)]^{-1}$. (B) Im[$Ni^{2+}(Gly_4-3H^+)]^{-1}$.

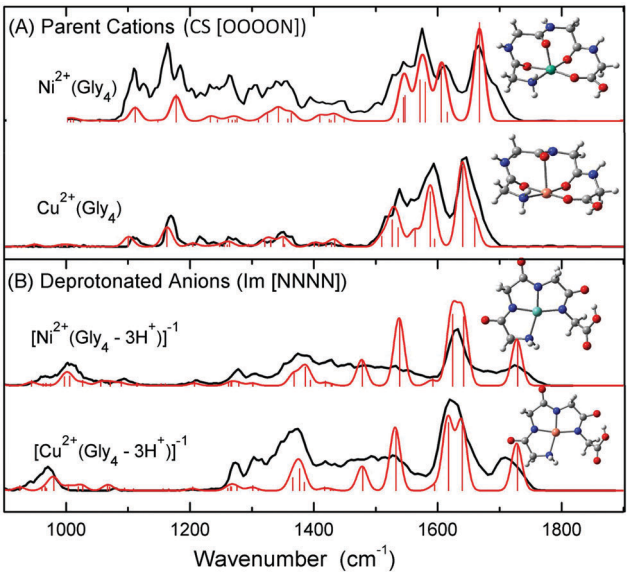

Fig. 7 Comparison of the spectra of the Gly_4 complexes (A) and the triply deprotonated Gly_4 complexes (B) of Ni(II) and Cu(II). The experimental IRMPD spectra (black) are plotted along with the best-fit computed spectrum (red). Computed spectra (red) are for CS[OOOON] for the parent cations and Im[NNNN] for the deprotonated anions.

extremely broadened in the experimental IRMPD spectrum. Considering the two calculated modes in this region, both involve large motions of atoms participating in the hydrogen bonding of the carboxyl proton, perhaps indicative of a shared proton.[98,99] The mode near 1540 cm^{-1} is the red-shifted amide I stretching motion of the hydrogen-bonded amide carbonyl oxygen, and the mode near 1480 cm^{-1} is a bending motion of the carboxyl proton. It is not surprising that both of these hydrogen-bonded modes would be severely broadened.

No equivalent of the fully CS configuration is possible for this deprotonated Gly_4 complex, but a reasonable structure with some CS character exists, labeled Im2CS1[NNON] in Fig. S7 (ESI†), having one CS-type amide carbonyl oxygen bound to the metal along with two deprotonated amide nitrogens and the terminal amino nitrogen. As the figure makes clear, this structure is ruled out both by its relatively high energy and by the lack of correspondence with its predicted spectrum. This comparison reemphasizes the preference of the nickel ion for coordination to deprotonated nitrogen ligands over amide carbonyl oxygens.

The Ala_3 complex similarly forms a triply deprotonated anionic complex (Fig. 6). As this structure is not complicated by a hydrogen-bonded (shared) proton, this complex shows an IRMPD spectrum corresponding well to the expected Im[NNON] structure with all of the available chelation points binding the metal in a low-spin square-planar array. No other structure type for this complex was found within 60 kJ mol^{-1}.

Comparison with Cu(II) complexes. In condensed phases, Ni(II) and Cu(II) show quite parallel behavior in their coordination properties, having similar propensities for square-planar binding to deprotonated amide nitrogens.[70,71] In order to compare the gas-phase behavior of the two metals, copper complexes were successfully formed from the electrospray source. In particular, it was interesting to see whether the unexpected CS structure for the $Ni^{2+}Gly_4$ complex is reproduced in the copper case.

The spectrum of the $Cu^{2+}Gly_4$ complex is shown in Fig. 7(A). It is seen to match convincingly with the predicted CS[OOOON] spectrum, with no indication of contributions from other structures, as is shown in more detail in Fig. S8 (ESI†). It is clearly parallel to the nickel case.

It would be expected that the same effects that encourage the transition from CS to Im type binding would operate equally for copper complexes as for nickel complexes. This expectation is realized in the case of outright deprotonation as well, as illustrated by the spectrum of the triply deprotonated $[Cu^{2+}(Gly_4-3H^+)]^-$ complex shown in Fig. 7(B). The spectra of the nickel and copper complexes are very similar, confirming that the structures are similar. Comparison with a few low-energy alternatives in Fig. S9 (ESI†) gives additional support to assigning the structure as Im[NNNN]. (The Im[NNNO] structure actually gives a slightly better spectroscopic fit in the 1700 cm^{-1} region, but this structure is much higher in energy, and does not account for the features around 1500 cm^{-1} and 980 cm^{-1}, so it is firmly rejected.) The extreme broadening of the features in the 1450 to 1600 cm^{-1} region is similar to that observed for the nickel complex.

Structures and spin states. The all-or-none principle for Ni^{2+} complexation (whereby the polydentate ligand coordinates either with all of the potentially coordinated amide nitrogens having metal-to-deprotonated-nitrogen bonds, or else with no amide nitrogens having such rearrangements) has been considered as a useful generalization in solid and solution phases.[68,77,80] The present results suggest that such a principle may not be universal in the gas phase, as shown by the very favorable relative stability of the Im2CS1 conformations demonstrated experimentally for FGGF (Fig. S2, ESI†), and shown computationally for both FGGF (Fig. S2, ESI†) and for the second-most-favorable structure for Gly_4 (Fig. S1, ESI†). Except for the two dipeptides where planar four-coordinate binding is not available, the Im[NNON] pattern is the most stable of the possible iminol binding conformations, even for the tetrapeptides, where only the two amide linkages nearest the N-terminus are favored to undergo iminol

rearrangement while the third (C-terminal) amide linkage remains in amido form, not metal bound.

Ni(II) has the choice of low (singlet) or high (triplet) spin states for its complexes. The IRMPD spectra for the present set of ligands generally do not give a very clear distinction between these, the calculated singlet and triplet spectra for a particular conformation of the ligand usually being quite similar. Fig. S1, S3, S5 and S6 (ESI†) show illustrative examples of this similarity by displaying both singlet and triplet spectra predicted for the same conformation. (Note that in all cases the singlet and triplet calculations of a given conformation are independently optimized.) As found for these examples, along with numerous other cases not shown here, it would not be easy to decide whether a given conformation is favored to be singlet or triplet based only on comparison of the two predictions with the observed IRMPD spectrum. However, the calculated thermochemistry is typically very different for a given structure pair. For the examples discussed in this report, the thermochemical calculations of the ground states strongly indicate that low (singlet) spin is preferred for all of the Im3 and Im2CS1 complexes, *i.e.* for the ground-state conformations of all of the present examples except the Gly_4 complexes. By contrast, high spin (triplet) is preferred over singlet spin for the (CS) penta-coordinate Ni(II)Gly_4 complex.

The energy calculations of low-lying conformations for the tri- and tetrapeptide complexes (leaving aside the different situation for the triply deprotonated complexes) also suggest some further spin-state generalizations, independent of the question of whether the ground state is Im or CS. The low-lying four-coordinate square-planar conformations favor singlet spin by roughly 60 kJ mol^{-1} relative to the triplet state having the same structure. This is in line with the solution-phase generalization that the square-planar nickel complexes are low-spin. On the other hand, all of the low-lying conformations having CS-type metal binding favor triplet spin compared with corresponding singlet calculations of the same structures, usually by more than 100 kJ mol^{-1} (although for the Gly_4 complex the triplet CS[OOOON] structure is only 39 kJ mol^{-1} more stable than the singlet CS[OOOON] structure).

It will be interesting to see in future work how these generalizations about preferred binding patterns and spin states play out for larger peptides.

4. Conclusions

As is generally the case in the condensed phase, the peptide complexation behavior of Cu^{2+} in the gas phase is found to be closely analogous to Ni^{2+}. The surprising result that the parent-ion nickel complex with tetraglycine has definite CS binding is reproduced in the copper case. The expected result of square-planar Im binding for the triply deprotonated anion complex of the copper ion with tetraglycine is also strongly confirmed experimentally.

The present gas-phase results support the principle that Ni(II) in peptide complexes, notably in biological environments, can favor either CS-type or iminol-type binding sites, depending on the local driving force toward backbone deprotonation processes. The present gas-phase modeling exemplifies the playing out of conflicting influences in determining the preference for one or the other binding pattern. The simple CS complexes of Ni(II) and Cu(II) with Gly_4 show that pentacoordination of the metal ion involving multiple C═O chelation sites can be favorable. However, the balance can tip in favor of tetracoordinate square-planar Im binding by (a) the introduction of hydrogen-bonding possibilities involving active side chains, (b) shortage of C═O chelation sites allowing stronger metal–nitrogen bonds to predominate, or (c) active deprotonation of amide nitrogens by outright proton stripping, as illustrated here by the triply deprotonated ions.

In condensed phase environments, the ATCUN binding pattern for Cu(II) and Ni(II) in transporter/storage proteins of the serum albumin family is a notable example of the deprotonated-nitrogen motif,[67–71] as is the large literature of deprotonated-amide binding in solution-phase small-peptide organometallic complexes.[65,68,69,76–82] Monomeric Ni(II) sites in enzymes are relatively unusual, but several are known which provide examples of nature's preferences for the structure of such sites. Eight enzymatic systems are accepted as having capability and selectivity for Ni(II) binding,[100] three of which have an isolated, monomeric Ni(II) ion. Two of these three (bacterial glyoxylase I[101] and acireductone dioxygenase (ARD))[100] coordinate in high-spin octahedral geometry, analogous to the gas-phase CS binding mode discussed here. The third of these, superoxide dismutase (SOD), uses two cysteine sulfur chelation points along with imidazole nitrogens to form a low-spin square-planar site. It is interesting that the two enzymes (glyoxylase I and ARD) having nitrogen and oxygen chelating ligands adopt a high-spin octahedral form analogous to our gas-phase CS conformation, which we hypothesize to be a favorable conformation for Ni(II) in the absence of other factors pushing toward backbone deprotonation.

Acknowledgements

This work was financially supported by the ''Nederlandse Organisatie voor Wetenschappelijk Onderzoek'' (NWO). RCD acknowledges support from the National Science Foundation, Grant PIRE-0730072, and expresses gratitude to the FELIX facility for its continuing welcome. The FELIX staff, and particularly Dr Lex van der Meer and Dr Britta Redlich, are gratefully acknowledged for their assistance. We thank SURFsara Computing and Networking Services (www.surfsara.nl) for their support in using the Lisa Compute Cluster. This study was made possible by the FELIX infrastructure.

References

1 R. C. Dunbar, G. Berden, J. K. Martens and J. Oomens, *J. Phys. Chem. A*, 2015, **119**, 9901–9909.
2 R. C. Dunbar, G. Berden and J. Oomens, *Int. J. Mass Spectrom.*, 2013, **354**, 356–364.

3 R. C. Dunbar, J. Oomens, G. Berden, J. K. C. Lau, U. H. Verkerk, A. C. Hopkinson and K. W. M. Siu, *J. Phys. Chem. A*, 2013, **117**, 5335–5343.
4 R. C. Dunbar, N. C. Polfer, G. Berden and J. Oomens, *Int. J. Mass Spectrom.*, 2012, **330–332**, 71–77.
5 R. C. Dunbar, J. D. Steill, N. C. Polfer, G. Berden and J. Oomens, *Angew. Chem., Int. Ed.*, 2012, **51**, 4591–4593.
6 F. Lanucara, S. W. Holman, C. J. Gray and C. E. Eyers, *Nat. Chem.*, 2014, **6**, 281–294.
7 L. Konermann, J. F. Pan and Y. H. Liu, *Chem. Soc. Rev.*, 2011, **40**, 1224–1234.
8 F. O. Talbot, A. Rullo, H. Yao and R. A. Jockusch, *J. Am. Chem. Soc.*, 2010, **132**, 16156–16164.
9 O. P. Balaj, C. Kapota, J. Lemaire and G. Ohanessian, *Int. J. Mass Spectrom.*, 2008, **269**, 196–209.
10 O. P. Balaj, D. Semrouni, V. Steinmetz, E. Nicol, C. Clavaguera and G. Ohanessian, *Chem. – Eur. J.*, 2012, **18**, 4583–4592.
11 B. Bellina, I. Compagnon, L. MacAleese, F. Chirot, J. Lemoine, P. Maitre, M. Broyer, R. Antoine, A. Kulesza, R. Mitric, V. Bonacic-Koutecky and P. Dugourd, *Phys. Chem. Chem. Phys.*, 2012, **14**, 11433–11440.
12 B. J. Bythell, U. Erlekam, B. Paizs and P. Maitre, *ChemPhysChem*, 2009, **10**, 883–885.
13 B. J. Bythell, P. Maitre and B. Paizs, *J. Am. Chem. Soc.*, 2010, **132**, 14766–14779.
14 C. F. Correia, C. Clavaguera, U. Erlekam, D. Scuderi and G. Ohanessian, *ChemPhysChem*, 2008, **9**, 2564–2573.
15 R. C. Dunbar, J. Steill, N. C. Polfer and J. Oomens, *J. Phys. Chem. B*, 2009, **113**, 10552–10554.
16 R. C. Dunbar, J. D. Steill and J. Oomens, *Int. J. Mass Spectrom.*, 2010, **297**, 107–115.
17 R. C. Dunbar, J. D. Steill and J. Oomens, *J. Am. Chem. Soc.*, 2011, **133**, 9376–9386.
18 S. Durand, M. Rossa, O. Hernandez, B. Paizs and P. Maitre, *J. Phys. Chem. A*, 2013, **117**, 2508–2516.
19 U. Erlekam, B. J. Bythell, D. Scuderi, M. Van Stipdonk, B. Paizs and P. Maitre, *J. Am. Chem. Soc.*, 2009, **131**, 11503–11508.
20 G. Frison, G. van der Rest, F. Turecek, T. Besson, J. Lemaire, P. Maitre and J. Chamot-Rooke, *J. Am. Chem. Soc.*, 2008, **130**, 14916–14917.
21 K. Joshi, D. Semrouni, G. Ohanessian and C. Clavaguera, *J. Phys. Chem. B*, 2012, **116**, 483–490.
22 J. K. Martens, I. Compagnon, E. Nicol, T. B. McMahon, C. Clavaguera and G. Ohanessian, *J. Phys. Chem. Lett.*, 2012, **3**, 3320–3324.
23 J. Oomens, N. Polfer, D. T. Moore, L. van der Meer, A. G. Marshall, J. R. Eyler, G. Meijer and G. von Helden, *Phys. Chem. Chem. Phys.*, 2005, **7**, 1345–1348.
24 B. Paizs, B. J. Bythell and P. Maitre, *J. Am. Soc. Mass Spectrom.*, 2012, **23**, 664–675.
25 N. C. Polfer, J. Oomens and R. C. Dunbar, *ChemPhysChem*, 2008, **9**, 579–589.
26 N. C. Polfer, B. Paizs, L. C. Snoek, I. Compagnon, S. Suhai, G. Meijer, G. von Helden and J. Oomens, *J. Am. Chem. Soc.*, 2005, **127**, 8571–8579.
27 J. S. Prell, M. Demireva, J. Oomens and E. R. Williams, *J. Am. Chem. Soc.*, 2009, **131**, 1232–1242.
28 J. S. Prell, T. G. Flick, J. Oomens, G. Berden and E. R. Williams, *J. Phys. Chem. A*, 2010, **114**, 854–860.
29 D. Semrouni, O. P. Balaj, F. Calvo, C. F. Correia, C. Clavaguera and G. Ohanessian, *J. Am. Soc. Mass Spectrom.*, 2010, **21**, 728–738.
30 B. Bellina, I. Compagnon, L. Joly, F. Albrieux, A. R. Allouche, F. Bertorelle, J. Lemoine, R. Antoine and P. Dugourd, *Int. J. Mass Spectrom.*, 2010, **297**, 36–40.
31 Y. M. E. Fung, T. Besson, J. Lemaire, P. Maitre and R. A. Zubarev, *Angew. Chem., Int. Ed.*, 2009, **48**, 8340–8342.
32 J. Oomens and J. D. Steill, *J. Am. Soc. Mass Spectrom.*, 2010, **21**, 698–706.
33 J. C. Poully, G. Gregoire, R. Ballivian, P. Dugourd and J. P. Schermann, *Vib. Spectrosc.*, 2011, **56**, 105–109.
34 R. Antoine and P. Dugourd, *Phys. Chem. Chem. Phys.*, 2011, **13**, 16494–16509.
35 C. Brunet, R. Antoine, A. R. Allouche, P. Dugourd, F. Canon, A. Giuliani and L. Nahon, *J. Phys. Chem. A*, 2011, **115**, 8933–8939.
36 L. Joly, R. Antoine, F. Albrieux, R. Ballivian, M. Broyer, F. Chirot, J. Lemoine, P. Dugourd, C. Greco, R. Mitric and V. Bonacic-Koutecky, *J. Phys. Chem. B*, 2009, **113**, 11293–11300.
37 L. Joly, R. Antoine, A. R. Allouche, M. Broyer, J. Lemoine and P. Dugourd, *J. Phys. Chem. A*, 2009, **113**, 6607–6611.
38 B. B. Kirk, A. J. Trevitt, S. J. Blanksby, Y. Tao, B. N. Moore and R. R. Julian, *J. Phys. Chem. A*, 2013, **117**, 1228–1232.
39 G. Papadopoulos, A. Svendsen, O. V. Boyarkin and T. R. Rizzo, *Far. Disc.*, 2011, **150**, 243–255.
40 G. Papadopoulos, A. Svendsen, O. V. Boyarkin and T. R. Rizzo, *J. Am. Soc. Mass Spectrom.*, 2012, **23**, 1173–1181.
41 J. A. Stearns, O. V. Boyarkin and T. R. Rizzo, *J. Am. Chem. Soc.*, 2007, **129**, 13820–13821.
42 T. N. Wassermann, O. V. Boyarkin, B. Paizs and T. R. Rizzo, *J. Am. Soc. Mass Spectrom.*, 2012, **23**, 1029–1045.
43 Y. M. Xie, H. F. Schaefer, R. Silaghi-Dumitrescu, B. Peng, Q. S. Li, J. A. Stearns and T. R. Rizzo, *Chem. – Eur. J.*, 2012, **18**, 12941–12944.
44 B. Bellina, I. Compagnon, S. Houver, P. Maitre, A. R. Allouche, R. Antoine and P. Dugourd, *Angew. Chem., Int. Ed.*, 2011, **50**, 11430–11432.
45 R. C. Dunbar, J. D. Steill, N. C. Polfer and J. Oomens, *Int. J. Mass Spectrom.*, 2009, **283**, 77–84.
46 M. Guidi, U. J. Lorenz, G. Papadopoulos, O. V. Boyarkin and T. R. Rizzo, *J. Phys. Chem. A*, 2009, **113**, 797–799.
47 P. Kupser, K. Pagel, J. Oomens, N. Polfer, B. Koksch, G. Meijer and G. von Helden, *J. Am. Chem. Soc.*, 2010, **132**, 2085–2093.
48 B. Lucas, G. Gregoire, J. Lemaire, P. Maitre, J. M. Ortega, A. Rupenyan, B. Reimann, J. P. Schermann and C. Desfrancois, *Phys. Chem. Chem. Phys.*, 2004, **6**, 2659–2663.
49 J. K. Martens, J. Grzetic, G. Berden and J. Oomens, *Int. J. Mass Spectrom.*, 2015, **377**, 179–187.
50 N. S. Nagornova, M. Guglielmi, M. Doemer, I. Tavernelli, U. Rothlisberger, T. R. Rizzo and O. V. Boyarkin, *Angew. Chem., Int. Ed.*, 2011, **50**, 5383–5386.

51 N. S. Nagornova, T. R. Rizzo and O. V. Boyarkin, *J. Am. Chem. Soc.*, 2010, **132**, 4040–4041.
52 N. S. Nagornova, T. R. Rizzo and O. V. Boyarkin, *Science*, 2012, **336**, 320–323.
53 N. S. Nagornova, T. R. Rizzo and O. V. Boyarkin, *Angew. Chem., Int. Ed.*, 2013, **52**, 6002–6005.
54 J. S. Prell, J. T. O'Brien, J. D. Steill, J. Oomens and E. R. Williams, *J. Am. Chem. Soc.*, 2009, **131**, 11442–11449.
55 J. A. Stearns, M. Guidi, O. V. Boyarkin and T. R. Rizzo, *J. Chem. Phys.*, 2007, **127**, 154322.
56 J. A. Stearns, C. Seaiby, O. V. Boyarkin and T. R. Rizzo, *Phys. Chem. Chem. Phys.*, 2009, **11**, 125–132.
57 K. Tanabe, M. Miyazaki, M. Schmies, A. Patzer, M. Schutz, H. Sekiya, M. Sakai, O. Dopfer and M. Fujii, *Angew. Chem., Int. Ed.*, 2012, **51**, 6604–6607.
58 R. H. Wu and T. B. McMahon, *J. Am. Chem. Soc.*, 2007, **129**, 11312–11313.
59 R. H. Wu and T. B. McMahon, *Chem. – Eur. J.*, 2008, **14**, 7765–7770.
60 M. B. Burt and T. D. Fridgen, *Eur. J. Mass Spectrom.*, 2012, **18**, 235–250.
61 J. R. Eyler, *Mass Spectrom. Rev.*, 2009, **28**, 448–467.
62 T. D. Fridgen, *Mass Spectrom. Rev.*, 2009, **28**, 586–607.
63 N. C. Polfer and J. Oomens, *Mass Spectrom. Rev.*, 2009, **28**, 468–494.
64 R. C. Dunbar in *Gas-Phase IR Spectroscopy and Structure of Biological Molecules*, ed. A. M. Rijs and J. Oomens, 2015, vol. 364, pp. 183–223.
65 R. B. Martin, M. Chamberlin and J. T. Edsall, *J. Am. Chem. Soc.*, 1960, **82**, 495–498.
66 R. Chattopadhyaya, W. E. Meador, A. R. Means and F. A. Quiocho, *J. Mol. Biol.*, 1992, **228**, 1177–1192.
67 C. Harford and B. Sarkar, *Acc. Chem. Res.*, 1997, **30**, 123–130.
68 H. Kozlowski, W. Bal, M. Dyba and T. Kowalik-Jankowska, *Coord. Chem. Rev.*, 1999, **184**, 319–346.
69 H. Kozlowski, S. Potocki, M. Remelli, M. Rowinska-Zyrek and D. Valensin, *Coord. Chem. Rev.*, 2013, **257**, 2625–2638.
70 H. Kozlowski, T. Kowalik-Jankowska and M. Jezowska-Bojczuk, *Coord. Chem. Rev.*, 2005, **249**, 2323–2334.
71 I. Sovago, E. Farkas, C. Bertalan, A. Lebkiri, T. Kowalik-Jankowska and H. Kozlowski, *J. Inorg. Biochem.*, 1993, **51**, 715–726.
72 T. Wyttenbach, D. Liu and M. T. Bowers, *J. Am. Chem. Soc.*, 2008, **130**, 5993–6000.
73 C. S. Burns, E. Aronoff-Spencer, C. M. Dunham, P. Lario, N. I. Avdievich, W. E. Antholine, M. M. Olmstead, A. Vrielink, G. J. Gerfen, J. Peisach, W. G. Scott and G. L. Millhauser, *Biochemistry*, 2002, **41**, 3991–4001.
74 F. Guerrieri, V. Minicozzi, S. Morante, G. Rossi, S. Furlan and G. La Penna, *J. Biol. Inorg. Chem.*, 2009, **14**, 361–374.
75 L. Quintanar, L. Rivillas-Acevedo, R. Grande-Aztatzi, C. Z. Gomez-Castro, T. Arcos-Lopez and A. Vela, *Coord. Chem. Rev.*, 2013, **257**, 429–444.
76 H. Sigel and R. B. Martin, *Chem. Rev.*, 1982, **82**, 385–426.
77 R. B. Martin in *Metal Ions in Biological Systems: Nickel and Its Role in Biology*, ed. A. Sigel and H. Sigel, Marcel Dekker, New York, 1988; vol. 23, pp. 123–164.
78 I. Sovago in *Ellis Horwood Series in Inorganic Chemistry: Biocoordination Chemistry: Coordination Equilibria in Biologically Active Systems*, ed. K. Burger, Ellis Hornwood, New York, 1990, pp. 135–184.
79 R. B. Martin in *Metal Ions in Biological Systems: Probing of Proteins by Metal Ions and their Low-Molecular-Weight Complexes*, ed. A. Sigel and H. Sigel, 2001, vol. 38, pp. 1–23.
80 I. Sovago and K. Osz, *Dalton Trans.*, 2006, 3841–3854.
81 T. Kowalik-Jankowska, H. Kozlowski, E. Farkas and I. Sovago, *Met. Ions Life Sci.*, John Wiley & Sons Ltd, 2007, vol. 2, pp. 63–107.
82 R. J. Sundberg and R. B. Martin, *Chem. Rev.*, 1974, **74**, 471–517.
83 M. J. Frisch, *et al.*, *Gaussian 09, Revision A.02*, Gaussian, Inc., Pittsburgh, PA, 2009. See ESI† for full reference.
84 T. E. Hofstetter, C. Howder, G. Berden, J. Oomens and P. B. Armentrout, *J. Phys. Chem. B*, 2011, **115**, 12648–12661.
85 D. Wang, K. Gulyuz, C. N. Stedwell, L. Yu and N. C. Polfer, *Int. J. Mass Spectrom.*, 2012, **330–332**, 144–151.
86 M. Swart, M. Solà and F. M. Bickelhaupt, *J. Chem. Phys.*, 2009, **131**, 094103.
87 M. Swart, A. W. Ehlers and K. Lammertsma, *Mol. Phys.*, 2004, **102**, 2467–2474.
88 S. Grimme, S. Ehrlich and L. Goerigk, *J. Comp. Chem.*, 2011, **32**, 1456–1465.
89 S. Grimme, J. Antony, S. Ehrlich and H. Krieg, *J. Chem. Phys.*, 2010, 154104.
90 W. L. Pearson, C. Contreras, D. Powell, G. Berden, J. Oomens, B. Bendiak and J. R. Eyler, *J. Phys. Chem. B*, 2015, **119**, 12970–12981.
91 G. C. Boles, R. A. Coates, G. Berden, J. Oomens and P. B. Armentrout, *J. Phys. Chem. B*, 2016, **119**, 11607–11617.
92 R. Sikari, S. Sinha, U. Jash, S. Das, P. Brandao, B. de Bruin and N. D. Paul, *Inorg. Chem.*, 2016, **55**, 4114.
93 A. G. Starikov, R. M. Minyaev and V. I. Minkin, *Chem. Phys. Lett.*, 2008, **459**, 27–32.
94 A. G. Starikov, R. M. Minyaev and V. I. Minkin, *THEOCHEM*, 2009, **895**, 138–141.
95 J. K. Martens, J. Grzetic, G. Berden and J. Oomens, *Nat. Commun.*, 2016, **7**, 11754.
96 P. Hu and M. L. Gross, *J. Am. Chem. Soc.*, 1993, **115**, 8821–8828.
97 P. B. Armentrout, M. T. Rodgers, J. Oomens and J. D. Steill, *J. Phys. Chem. A*, 2008, **112**, 2248–2257.
98 J. R. Roscioli, L. R. McCunn and M. A. Johnson, *Science*, 2007, **316**, 249–254.
99 C. L. Perrin and J. B. Nielson, *Annu. Rev. Phys. Chem.*, 1997, **48**, 511–544.
100 S. W. Ragsdale, *J. Biol. Chem.*, 2009, **284**, 18571–18575.
101 J. F. Honek, *Biochem. Soc. Trans.*, 2014, **42**, 479–484.

